Journal of Power Sources 268 (2014) 700–705

Contents lists available at ScienceDirect

Journal of Power Sources

journal homepage: www.elsevier.com/locate/jpowsour

Short communication

Template-free synthesis of vanadium oxides nanobelt arrays as high-rate cathode materials for lithium ion batteries

Mulan Qin [a], Qiang Liang [a], Anqiang Pan [a, *], Shuquan Liang [a, *], Qing Zhang [b], Yan Tang [a, c], Xiaoping Tan [a, c]

[a] School of Materials Science and Engineering, Central South University, Changsha 410083, Hunan, China
[b] School of Chemistry and Chemical Engineering, Central South University, Changsha 410083, Hunan, China
[c] Key Laboratory of the Ministry of Education, Changsha 410083, Hunan, China

HIGHLIGHTS

- VO_2 (B) nanobelt arrays have been synthesized by a template-free hydrothermal method.
- Porous V_2O_5 nanobelt arrays can be obtained by calcinating the VO_2 nanobelt arrays in air.
- The V_2O_5 nanobelt array electrode shows excellent rate capability and cyclic stability in lithium ion batteries.

GRAPHICAL ABSTRACT

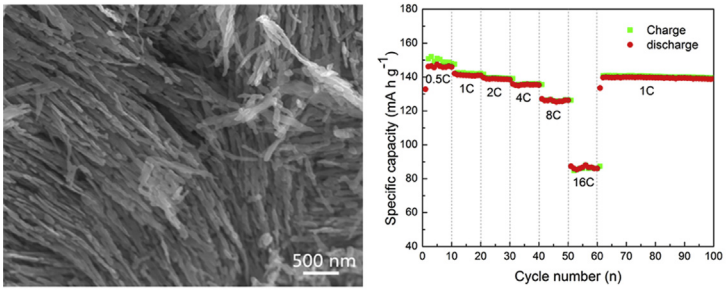

ARTICLE INFO

Article history:
Received 28 April 2014
Received in revised form
16 June 2014
Accepted 20 June 2014
Available online 7 July 2014

Keywords:
Lithium-ion battery
Ultra-thin nanobelts
Vanadium oxides
Cathode material

ABSTRACT

A facile hydrothermal route has been developed to fabricate the metastable VO_2 (B) ultra-thin nanobelt arrays, which can be converted into V_2O_5 porous nanobelt arrays after calcinating VO_2 (B) in air at 400 °C for 1 h. The influence of hydrothermal time to the crystallinity and morphology of the VO_2 phase has been studied. A possible mechanism for the formation of VO_2 nanobelt arrays has been proposed in this paper. As a cathode material for lithium ion batteries, the V_2O_5 nanobelt arrays show excellent rate capability and cycling stability. An initial discharge capacity of 142 mA h g^{-1} can be delivered at a current density of 50 mA g^{-1} with almost no capacity fading after 100 cycles. Even at a current density of 1000 mA g^{-1}, they still exhibit the capacity of 130 mA h g^{-1} and superior capacity retention capability. The excellent electrochemical properties are attributed to the ultra-thin thickness and the porous structures of the nanobelts.

1. Introduction

Because of their high energy density, good cycling stability and flexible design, lithium-ion batteries (LIBs) have been widely used in portable electronic devices, such as laptops and cell phones [1,2]. However, materials with higher capacity and better rate capability are urgently needed for the next-generation of LIBs, which are considered as power sources in the high power devices, such as hybrid electric vehicles (HEV) and electric vehicles (EV).

Vanadium pentoxide (V_2O_5) has attracted great attention as an alternative cathode material for LIBs mainly because of its high theoretical capacity (440 mA h g^{-1} for 3 Li^+ ions intercalation), easy synthesis, low cost and abundant in storage with respect to the

* Corresponding authors. Tel.: +86 0731 88836069; fax: +86 0731 88876692.
E-mail addresses: pananqiang@csu.edu.cn, pananqiang@gmail.com (A. Pan), lsq@mail.csu.edu.cn (S. Liang).

http://dx.doi.org/10.1016/j.jpowsour.2014.06.103
0378-7753/

commercial cathode $LiCoO_2$ [3]. However, the poor cycling stability [4] raised from its low diffusion coefficient of lithium ions (10^{-12}–10^{-15} cm^2 s^{-1}) [5] and moderate electronic conductivity (10^{-2}–10^{-3} S cm^{-1}) [6] hinders its development as a cathode material in LIBs. In the last decades, nanostructured materials have been demonstrated to have improved kinetics for Li^+ ions intercalation and de-intercalation process [4,6]. More attention has been paid to the fabrication of one-dimensional (1D) nanostructured vanadium oxides, such as nanorods [7,8], nanofibers [9,10], nanobelts [11,12], nanowires [13] and nanotubes [14], to improve their electrochemical performance as they can offer a range of unique advantages including large interfacial contact area between the electrode and electrolyte, short Li-ions transport distance, efficient 1D electron transport pathways and facile strain relaxation upon electrochemical cycling [7,8,11–18]. Although the rate capability is indeed greatly improved for these nanostructured vanadium oxides [4,14], the capacity retention capability is still need further improvement [19,20].

In this paper, we report a template-free hydrothermal method to synthesize ultra-thin VO_2 (B) nanobelt arrays with the thickness about 10 nm, which can be converted into V_2O_5 porous nanobelt arrays by calcining in air at 400 °C. The as-prepared V_2O_5 nanobelt arrays exhibit excellent rate capability and cycling stability.

2. Experimental

All the reagents and solvent were of analytical-grade and used without further purification. In a typical synthesis of VO_2 (B) nanobelts, 0.5 g V_2O_5 powders were added into 20 mL distilled water and magnetically stirred for 5 min to get the yellow slurry, which was then added with 10 mL ethylene glycol (EG). The mixture was sealed in Teflon-lined stainless steel autoclaves and maintained at 180 °C for different durations of 2, 6, 12, 18, 24 and 48 h. After cooling down to room temperature naturally, the deep-blue products were filtered off, washed with distilled water and absolute ethanol for several times before drying at 50 °C for 12 h in air. The obtained precipitates from the hydrothermal durations of 2, 6, 12 and 18 h were designated as VO_2-2 h, VO_2-6 h, VO_2-12 h and VO_2-18 h, respectively. V_2O_5 nanobelts were obtained by further calcining VO_2-12 h in air at 400 °C for 1 h with a heating rate of 2 °C min^{-1}.

The V_2O_5 nanobelts were assembled into coin-type cells (CR 2016) to evaluate their electrochemical properties. V_2O_5 active material, acetylene black and polyvinylidene fluoride (PVDF) binder in a weight ratio of 7:2:1 were dispersed in *N*-methyl-2-pyrrolidone (NMP) solution to make the slurry, which was coated on an aluminum foil and dried in a vacuum oven at 90 °C for 20 h to make the cathode. The half-cells were assembled in a glove box (Mbraun, Germany) filled with ultrahigh purity argon, using polypropylene membrane as the separator and 1 M $LiPF_6$ dissolved in ethylene carbonate/dimethyl carbonate (EC/DMC) = 1:1 (volume ratio) as the electrolyte. Cyclic voltammetry measurements were performed on a CHI 660C electrochemical workstation. The galvanostatic charge–discharge characteristics of the cells were recorded with a Land Battery Tester (Land CT 2001A, Wuhan, China) at room temperature, and the specific capacity is based on the weight of active material only. The loading of the active material was about 1–2 mg cm^2.

3. Results and discussion

Fig. 1a shows the XRD patterns of the hydrothermal products obtained under different reaction time. The diffraction peaks for VO_2-2 h, VO_2-6 h, VO_2-12 h and VO_2-18 h can be well indexed as

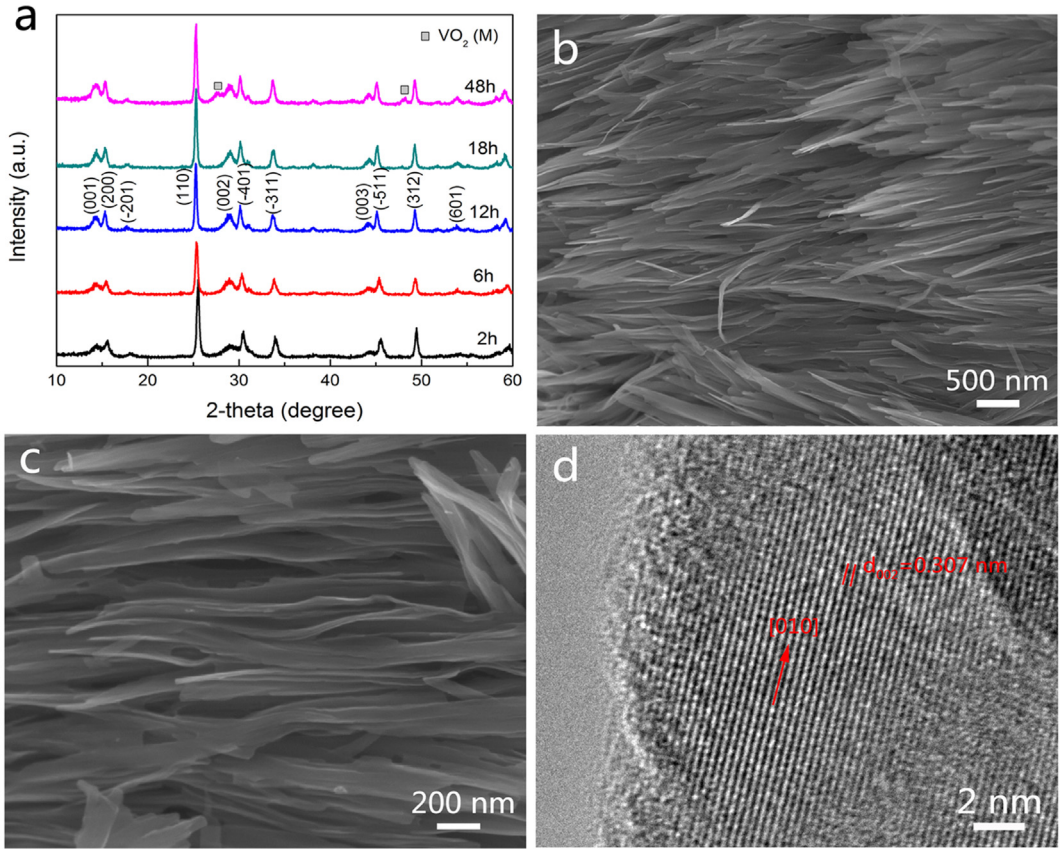

Fig. 1. (a) XRD patterns of the samples obtained at different time, (b, c) FESEM images and (d) HRTEM image of VO_2-12 h.

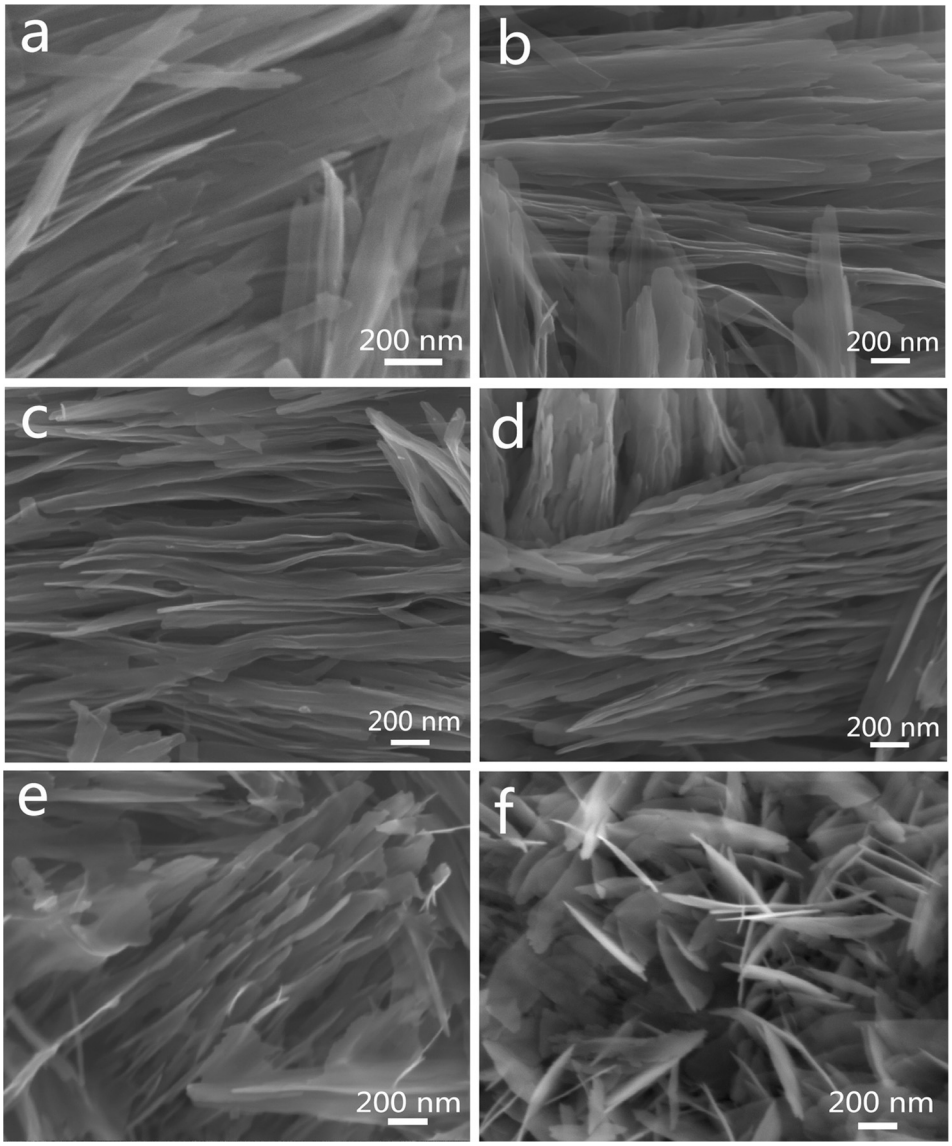

Fig. 2. FESEM images of vanadium oxides obtained at different times (a) 2 h, (b) 6 h, (c) 12 h, (d) 18 h, (e) 24 h and (f) 48 h.

metastable monoclinic VO_2 (B) (space group C2/m) with lattice parameters of $a = 11.989$ Å, $b = 3693$ Å and $c = 6.399$ Å, which are in good agreement with the reported values (JCPDS Card No. 31-1438, $a = 12.030$ Å, $b = 3.693$ Å and $c = 6.420$ Å) [21]. No impurity phase detected for VO_2-2 h indicates the VO_2 (B) nanobelts with high purity could be fastly fabricated within 2 h using the mixture solvent of ethylene glycol and distilled water (1:2, v/v). As shown in Fig. 1a, the metastable VO_2 phase is quite stable during the hydrothermal process from 2 h to 18 h. However, the metastable VO_2 (B) has the tendency of transferring into monoclinic VO_2 (M) indicated by the detection of the impurity phase of monoclinic VO_2 (M) at an extension hydrothermal time of 48 h. Moreover, the influence of the volume ratio of ethylene glycol and distilled water to the phases was investigated (see Fig. S1). The results indicate that the mixtures with the lower ratios are more beneficial to obtain the high purity of VO_2 (B) phase.

The morphologies of the VO_2-12 h are characterized by field-emission scanning electron microscope (FESEM). The FESEM images (Fig. 1b and c) reveal the product is composed of uniform nanobelts. It is interesting to find the nanobelts are parallel to each other to form the nanobelt arrays. The nanobelts are measured to have a thickness of about 10 nm, a width of about 200 nm and a length of about 2 μm. The clear lattice fringe of the high resolution TEM (HRTEM) image (Fig. 1d) indicates the good crystallinity of the nanobelts. The interplanar spacing of 0.307 nm is in good agreement with the distance of the neighboring (002) crystal planes of VO_2 (B), which indicates the individual VO_2 (B) nanobelt growth direction of [010].

The morphologies of the hydrothermal products prepared under different reaction time are studied by FESEM and the results are shown in Fig. 2. The nanobelts are all observed for the hydrothermal products under a series of 2, 6, 12 and 18 h. The result demonstrates that the VO_2 (B) can be easily obtained with good controllability. When the hydrothermal time extends to 24 and 48 h, the nanobelts become vertically aligned nanosheet arrays. The morphology changes may be caused by the new phase transition from VO_2 (B) to VO_2 (M), as proven by the XRD result (Fig. 1a).

The VO_2 nanobelt arrays can be converted into V_2O_5 nanobelt arrays after calcination in air at 400 °C for 1 h. The representative XRD pattern shown in Fig. 3a characterizes the phase purity and

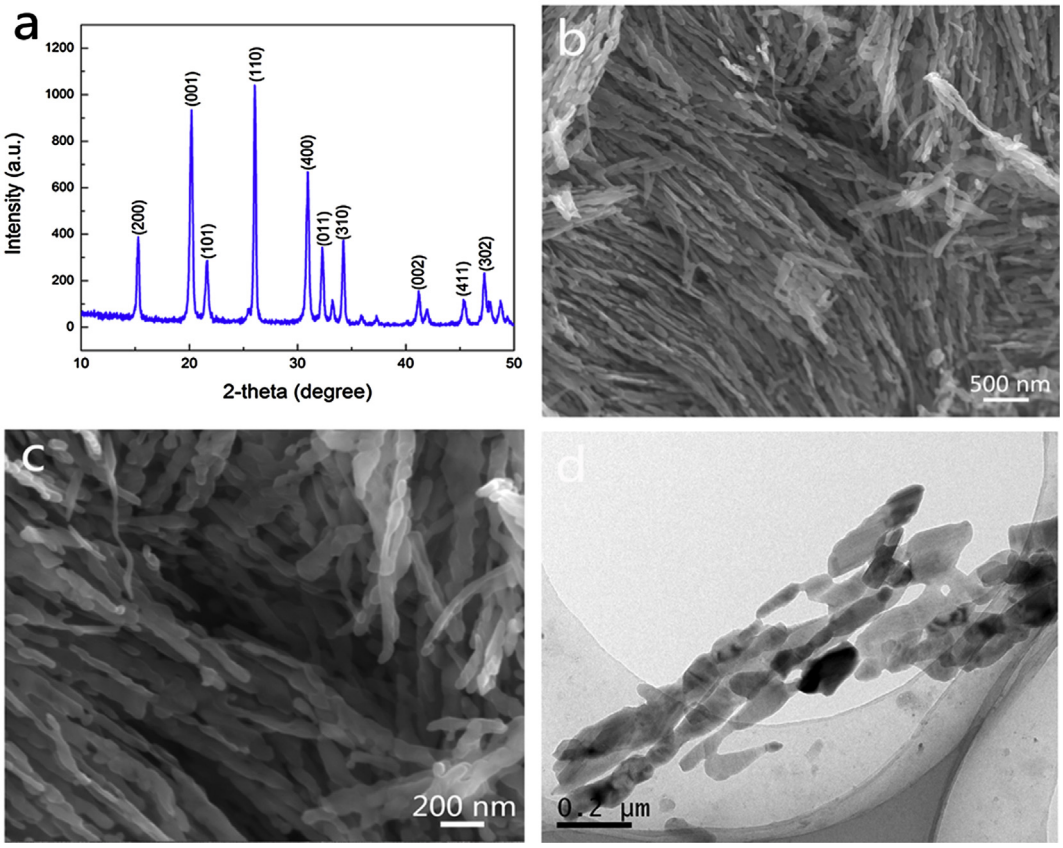

Fig. 3. (a) XRD patterns of V_2O_5 obtained from calcination of VO_2-12 h, (b, c) FESEM images and (d) TEM image of V_2O_5.

crystallinity of the obtained V_2O_5 nanobelt arrays. The XRD pattern can be perfectly indexed to the orthogonal V_2O_5 phase (JCPDS No. 41-1426, space group *Pmmn*, a = 11.516 Å, b = 3.566 Å and c = 3.777 Å) [22]. The morphologies and the detailed structure of V_2O_5 nanobelts were further investigated by FESEM and TEM. As shown in Fig. 3b, the nanobelt array structures are preserved after calcination for VO_2-12 h. The higher FESEM image (Fig. 3c) reveals the narrow thickness of about 20 nm and the length of about 2 μm for the nanobelts and the porous structure of the nanobelts. As shown in Fig. 3d, the nanobelts are composed of inter-connected nano-sized platelet particles and possess high porosity between the neighboring particles. The porous structure is believed to be created during the calcination process because of the atom reorganization from VO_2 (B) to V_2O_5.

The electrochemical properties of the porous V_2O_5 nanobelts were first evaluated by cyclic voltammetry. Fig. 4a shows the five consecutive cyclic voltammograms (CVs) of the electrode prepared from the porous nanobelts in the voltage range of 2.5–4 V vs. Li/Li^+. The observation of two well-defined current peaks at 3.37 and 3.17 V during the cathodic scan indicate the multi-step lithium ion intercalation process in the electrode materials, and the phases change from α-V_2O_5 to ε-$Li_{0.5}V_2O_5$ (3.37 V), and then to δ-LiV_2O_5 (3.17 V), consecutively [23,24]. The two anodic peaks at the potential of 3.25 and 3.45 V correspond to the lithium de-intercalation process and the successive backward transformation of the phases from δ-LiV_2O_5 to ε-$Li_{0.5}V_2O_5$, and α-V_2O_5, respectively [25,26]. The five CV curves are almost superimposed over each other, which indicate the high reversibility of the insertion/extraction reactions for the porous V_2O_5 nanobelts. Fig. 4b shows the charge–discharge curves of 1st, 10th, 20th, 50th and 100th cycles for the V_2O_5 electrode at a constant current density of 50 mA g^{-1} in the potential window from 2.5 to 4 V vs Li/Li^+. The specific discharge capacity is 142 mA h g^{-1}, 146 mA h g^{-1}, 146 mA h g^{-1}, 145 mA h g^{-1} and 141 mA h g^{-1}, respectively. The capacity fading rate is calculated to be 0.03% per cycle based, suggesting the excellent capacity retention. The discharge–charge plateaus correspond well with the peak positions shown on the CV curves (Fig. 4a). The cycling performance of the V_2O_5 electrodes at different current densities and the coulombic efficiency are shown in Fig. 4c. Very good capacity retentions and high coulombic efficiencies are observed from the 1st to the 100th cycles. The specific discharge capacity of 146 mA h g^{-1} is very close to the theoretical capacity of V_2O_5 crystallites electrodes (147 mA h g^{-1}). The Coulombic efficiency is nearly to 100%, suggesting the good reversibility for the Li-ions insertion/deinsertion process. Even at a much higher current density of 1000 mA g^{-1}, it can still have a specific discharge capacity of 130 mA h g^{-1} and retain the capacity of 128 mA h g^{-1} after 100 cycles. The capacity fading rate is calculated to be 0.015% per cycle, suggesting superior capacity retention capability. Fig. 4d shows the rate capability of the porous V_2O_5 nanobelt electrode. The electrode delivers the specific discharge capacities of 146 mAh g^{-1}, 142 mAh g^{-1}, 139 mAh g^{-1} and 135 mAh g^{-1} at 0.5C, 1C, 2C and 4C, respectively (1C = 147 mA g^{-1}). The specific discharge capacities of 127 mAh g^{-1} and 87 mA h g^{-1} can be still delivered when it is operated at 8C and 16C, respectively. After 60 cycles, the electrode can restore a specific discharge capacity of 140 mAh g^{-1} when the rate is reset to 1C. Negligible capacity fading from 140 mAh g^{-1} to 139 mAh g^{-1} was observed from the 60th to the 100th cycles. The electrochemical performance of V_2O_5 nanobelts is much better than that of previously reported V_2O_5 nanoparticles [23] and V_2O_5 microspheres [27]. The excellent rate performance and good capacity retention at various discharge rates are attributed to the

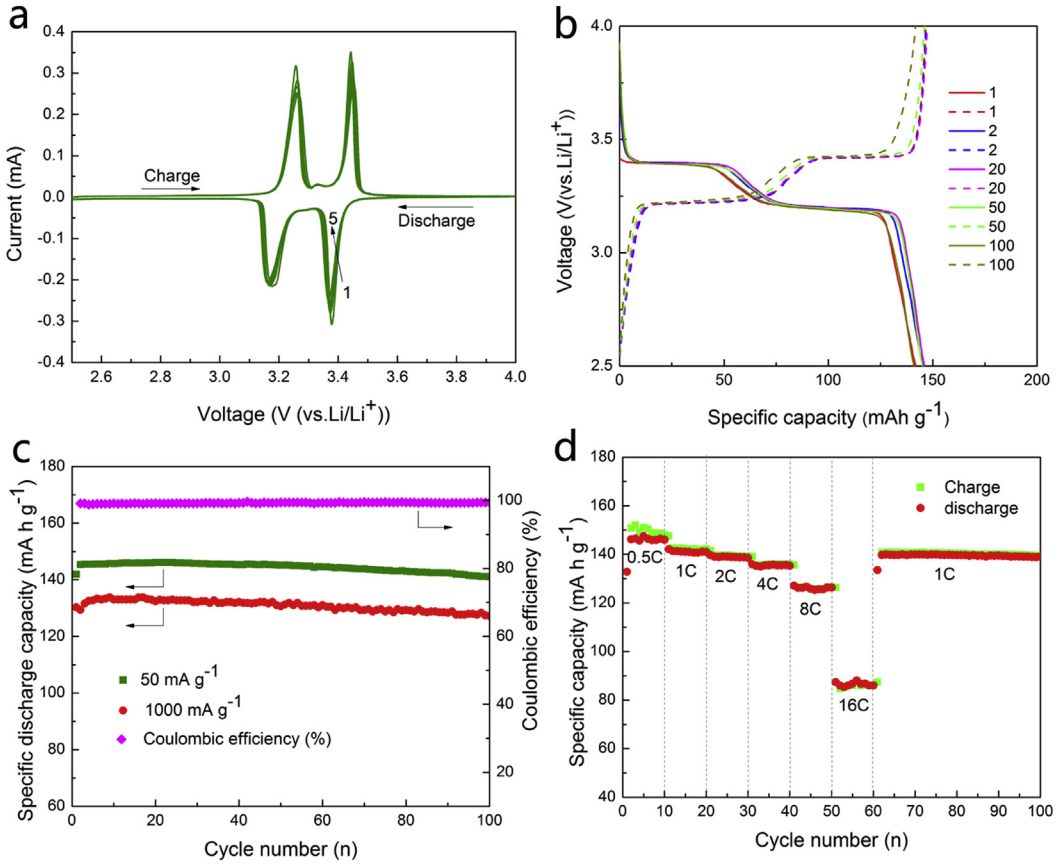

Fig. 4. (a) Cyclic voltammetric curves of V_2O_5 nanobelts electrodes at a scan rate of 0.05 mV s^{-1} between 2.5 V and 4 V vs. Li/Li^+. (b) Galvanostatic discharge/charge curves of V_2O_5 at the current density of 50 mA g^{-1}. (c) Cycling performance and coulombic efficiency of V_2O_5 at the different current density and (d) rate performance of V_2O_5 electrodes. Here 1C = 147 mA g^{-1}.

interesting porous V_2O_5 nanobelt arrays structures. The nano-sized nanobelts reduce the distance for Li-ions diffusion and the electron transportation. Moreover, the porous structures of the nanobelts arrays (shown in Fig. 3c and d) would facilitate the electrolyte penetration and increase the contact area between the active material and the electrolyte. Furthermore, the porous structure might be also of advantage to accommodate the volume variations during the Li-ions intercalation and deintercalation. The cost-effective preparation procedure and the excellent electrochemical performance electrode make the porous V_2O_5 nanobelt arrays promising alternative cathode materials for lithium ion batteries.

4. Conclusion

In summary, we have successfully synthesized metastable VO_2 (B) ultra-thin nanobelt arrays by a template-free hydrothermal approach. After calcination in air, they can be converted into porous V_2O_5 nanobelt arrays. As a cathode material for lithium ion batteries, the porous V_2O_5 nanobelt arrays show excellent rate performance and cycling stability. The good performance is attributed to the novel porous nanobelt array structures of V_2O_5, which can reduce the lithium ion diffusion and electron transportation distance, facilitate the electrolyte penetration and accommodate the volume changes upon cycling.

Acknowledgment

This work was supported by Creative Research Group of National Natural Science Foundation of China (50721003), National Natural Science Foundation of China (No. 51374255, 51202323), and the Fundamental Research Funds for the Central Universities of Central South University (2013zzts019).

Appendix A. Supplementary data

Supplementary data related to this article can be found at http://dx.doi.org/10.1016/j.jpowsour.2014.06.103.

References

[1] J.M. Tarascon, M. Armand, Nature 414 (2001) 359–367.
[2] B. Scrosati, J. Garche, J. Power Sources 195 (2010) 2419–2430.
[3] Y. Wang, G. Cao, Chem. Mater. 18 (2006) 2787–2800.
[4] Y. Wang, G. Cao, Adv. Mater. 20 (2008) 2251–2269.
[5] J.M. McGraw, C.S. Bahn, P.A. Parilla, J.D. Perkins, D.W. Readey, D.S. Ginley, Electrochim. Acta 45 (1999) 187–196.
[6] Y. Wang, K. Takahashi, K. Lee, G. Cao, Adv. Funct. Mater. 16 (2006) 1133–1144.
[7] K. Takahashi, S.J. Limmer, Y. Wang, G. Cao, J. Phys. Chem. B 108 (2004) 9795–9800.
[8] A. Pan, J.G. Zhang, Z. Nie, G. Cao, B.W. Arey, G. Li, S. Liang, J. Liu, J. Mater. Chem. 20 (2010) 9193–9199.
[9] Y.L. Cheah, N. Gupta, S.S. Pramana, V. Aravindan, G. Wee, M. Srinivasan, J. Power Sources 196 (2011) 6465–6472.
[10] E.A. Ponzio, T.M. Benedetti, R.M. Torresi, Electrochim. Acta 52 (2007) 4419–4427.
[11] G. Li, S. Pang, L. Jiang, Z. Guo, Z. Zhang, J. Phys. Chem. B 110 (2006) 9383–9386.
[12] Y. Wang, H.J. Zhang, K.W. Siah, C.C. Wong, J. Lin, A. Borgna, J. Mater. Chem. 21 (2011) 10336–10341.
[13] F. Zhou, X. Zhao, Y. Liu, C. Yuan, L. Li, Eur. J. Inorg. Chem. (2008) 2506–2509.
[14] Y. Wang, K. Takahashi, H. Shang, G. Cao, J. Phys. Chem. B 109 (2005) 3085–3088.
[15] X. Li, X. Chen, X. Chen, C. Han, C. Shi, J. Cryst. Growth 309 (2007) 43–47.

[16] G. Armstrong, J. Canales, A.R. Armstrong, P.G. Bruce, J. Power Sources 178 (2008) 723–728.
[17] L. Kong, Z. Liu, M. Shao, Q. Xie, W. Yu, Y. Qian, J. Solid State Chem. 177 (2004) 690–695.
[18] J. Liu, Q. Li, T. Wang, D. Yu, Y. Li, Angew. Chem. 116 (2004) 5158–5162.
[19] L. Mai, L. Xu, C. Han, X. Xu, Y. Luo, S. Zhao, Nano Lett. 10 (2010) 4750–4755.
[20] Y.G. Guo, J.S. Hu, L.J. Wan, Adv. Mater. 20 (2008) 2878–2887.
[21] C. Tsang, A. Manthiram, J. Electrochem. Soc. 144 (1997) 520–524.
[22] A. Pan, H.B. Wu, L. Yu, T. Zhu, X.W. Lou, Appl. Mater. Interfaces 4 (2012) 3874–3879.
[23] S.H. Ng, T.J. Patey, R. Büchel, F. Krumeich, J.Z. Wang, H.K. Liu, S.E. Pratsinis, P. Novák, Phys. Chem. Chem. Phys. 11 (2009) 3748–3755.
[24] S. Wang, S. Li, Y. Sun, X. Feng, C. Chen, Energy Environ. Sci. 4 (2011) 2854–2857.
[25] A. Odani, V.G. Pol, S.V. Pol, M. Koltypin, A. Gedanken, D. Aurbach, Adv. Mater. 18 (2006) 1431–1436.
[26] J.S. Braithwaite, C.R.A. Catlow, J.D. Gale, J.H. Harding, Chem. Mater. 11 (1999) 1990–1998.
[27] S. Wang, Z. Lu, D. Wang, C. Li, C. Chen, Y. Yin, J. Mater. Chem. 21 (2011) 6365–6369.